

Contents lists available at ScienceDirect

# Water Research

journal homepage: www.elsevier.com/locate/watres





# Electrochemical nutrient removal from natural wastewater sources and its impact on water quality

László Kékedy-Nagy <sup>a, b</sup>, Leah English <sup>c</sup>, Zahra Anari <sup>a, d</sup>, Mojtaba Abolhassani <sup>a</sup>, Bruno G. Pollet <sup>e, f</sup>, Jennie Popp <sup>c</sup>, Lauren F. Greenlee <sup>a, d, \*</sup>

- <sup>a</sup> Ralph E. Martin Department of Chemical Engineering, University of Arkansas, 3202 Bell Engineering Center, Fayetteville AR 72701, United States
- <sup>b</sup> Department of Electrical and Computer Engineering, Concordia University, Center of Structural and Functional Genomics, 7141 Sherbrooke St. West, Montreal H4B 1R6, Canada
- c Department of Agricultural Economics and Agribusiness, University of Arkansas, 217 Agriculture Building, Fayetteville, AR 72701, United States
- d Department of Chemical Engineering, Pennsylvania State University, 121 Chemical and Biomedical Engineering Building, University Park, PA 16802 United States
- <sup>e</sup> Hydrogen Energy and Sonochemistry research group, Department of Energy and Process Engineering, Faculty of Engineering, Norwegian University of Science and Technology (NTNU), NO-7491 Trondheim, Norway
- f Green Hydrogen Lab, Hydrogen Research Institute, Université du Québec à Trois-Rivières, 3351 Boulevard des Forges, Trois-Rivières, Québec G9A 5H7, Canada

#### ARTICLE INFO

#### Keywords: Electrochemistry Magnesium Corrosion Natural wastewater Nutrient removal

#### ABSTRACT

In this study, a suite of natural wastewater sources is tested to understand the effects of wastewater composition and source on electrochemically driven nitrogen and phosphorus nutrient removal. Kinetics, electrode behavior, and removal efficiency were evaluated during electrochemical precipitation, whereby a sacrificial magnesium (Mg) anode was used to drive precipitation of ammonium and phosphate. The electrochemical reactor demonstrated fast kinetics in the natural wastewater matrices, removing up to 54% of the phosphate present in natural wastewater within 1 min, with an energy input of only 0.04 kWh.m<sup>-3</sup>. After 1 min, phosphate removal followed a zero-order rate law in the 1 min - 30 min range. The zero-order rate constant (k) appears to depend upon differences in wastewater composition, where a faster rate constant is associated with higher Cl and NH4+ concentrations, lower Ca<sup>2+</sup> concentrations, and higher organic carbon content. The sacrificial Mg anode showed the lowest corrosion resistance in the natural industrial wastewater source, with an increased corrosion rate  $(v_{corr})$  of 15.8 mm.y<sup>-1</sup> compared to 1.9–3.5 mm.y<sup>-1</sup> in municipal wastewater sources, while the Tafel slopes  $(\beta)$ showed a direct correlation with the natural wastewater composition and origin. An overall improvement of water quality was observed where important water quality parameters such as total organic carbon (TOC), total suspended solids (TSS), and turbidity showed a significant decrease. An economic analysis revealed costs based upon experimental Mg consumption are estimated to range from 0.19 \$.m<sup>-3</sup> to 0.30 \$.m<sup>-3</sup>, but costs based upon theoretical Mg consumption range from 0.09 \$.m<sup>-3</sup> to 0.18 \$.m<sup>-3</sup>. Overall, this study highlights that water chemistry parameters control nutrient recovery, while electrochemical treatment does not directly produce potable water, and that economic analysis should be based upon experimentally-determined Mg consumption

**Synopsis Statement:** Magnesium-driven electrochemical precipitation of natural wastewater sources enables fast kinetics for phosphate removal at low energy input.

#### 1. Introduction

Agro-industrial and municipal wastewater effluents are well-known for their high levels of nutrients like phosphorus (P), nitrogen (N), or organic matter; therefore, it is crucial to treat these effluents before they are discharged into receiving water bodies to minimize potential environmental impacts and water quality problems on a global scale (Rasmussen et al., 2018; Tilman et al., 2011). Phosphorus is a non-renewable resource, where the majority is mined from rock phosphate, and its geographic concentration may generate compelling political or economic risks for many countries (Godfray et al., 2010). As the supply of rock phosphate steadily decreases, the costs of fertilizers will

E-mail address: greenlee@psu.edu (L.F. Greenlee).

<sup>\*</sup> Corresponding author.

increase, significantly impacting the affordability of food products (Cordell et al., 2009). Consequently, alternative sources for P should be considered with the emphasis on recyclable or reusable sources from various wastes to facilitate a sustainable global supply of P.

Researchers have shown the possibility to recover P from various waste sources in the form of a precipitate known as struvite (MgNH<sub>4</sub>PO<sub>4×</sub>6H<sub>2</sub>O or MAP), a white, orthorhombic, poorly soluble crystal, and a premium grade slow-release fertilizer (Massey et al., 2009; Shu et al., 2006; Zhang et al., 2019). Promising technologies such as electrically conducting membranes (Kekre et al., 2020), microbial fuel cells (MFCs) (Cusick and Logan, 2012; Fischer et al., 2011; Ichihashi and Hirooka, 2012), electrocoagulation (Dura and Breslin, 2019; Kim et al., 2018; Nasr et al., 2016), or electrochemical precipitation (Govindan et al., 2021; Hug and Udert, 2013; Kékedy-Nagy et al., 2020a, 2019, 2020b; Kruk et al., 2014; Li et al., 2021; Lin et al., 2018; Ren et al., 2017) have been proposed as feasible alternatives to existing technologies (Abel-Denee et al., 2018; Shu et al., 2019; Wang et al., 2019b; Zeng et al., 2018). To facilitate electrochemical precipitation, a Mg-based sacrificial anode provides the required amount of Mg in the form of Mg<sup>2+</sup> through anodic dissolution (corrosion), with an applied overpotential  $(\eta)$  to drive the struvite precipitation reaction.

The electrochemical behavior of Mg-based electrodes is complex and still not fully understood; controversy still exists about the corrosion and passivation processes of magnesium in general. Due to the very negative standard reduction potential of the Mg/Mg<sup>2+</sup> redox couple ( $E^{\emptyset}_{Mg/Mg2+}$ = -2.372 V vs. SHE) (Coates, 1945) and non-inert material characteristics, the anodic dissolution of Mg<sup>2+</sup> in solutions can be best described by a heterogeneous electron transfer coupled with or followed by a homogenous chemical (EC) reaction. Although the electrochemical behavior of Mg-based electrodes has been greatly studied in a wide range of aqueous solutions, the water composition has been usually well-defined or synthetic and most of these studies have been performed on a bench-scale (Belarbi and Trembly, 2018; Curioni et al., 2015; Liao et al., 2020; Liu et al., 2019; Wu et al., 2019). Moreover, these studies were mainly focused on Mg corrosion (Esmaily et al., 2017), P recovery (Cai et al., 2020), struvite production efficiency (Kékedy-Nagy et al., 2020b), and energy input based upon the Mg anode type used (Lei et al., 2020).

On the other hand, systematic studies regarding the general electrochemical behavior of the anode in complex matrixes such as raw industrial or municipal wastewater effluents are still lacking. In particular, there are a few studies available that compare how the electrochemical system performs across a suite of wastewater sources, where a comparison of water chemistry differences is possible due to the wastewater sources being treated by the same electrochemical system and setup. In addition, detailed studies regarding the impact of electrochemistry on the overall water quality after the electrochemical nutrient removal process by either a single cell batch reactor or a flow reactor have been generally avoided. Studies have typically focused on the performance of the electrochemical system to remove ammonia and phosphate, but have not analyzed a wide range of water chemistry parameters (Gao et al., 2020; Lei et al., 2019, 2021; Naresh Kumar et al., 2019; Ren et al., 2017; Tan et al., 2020; Wang et al., 2019a, 2019c). Our study thus attempts to fill an important knowledge gap on the importance of wastewater source water chemistry in understanding how the Mg-electrode based electrochemical system performs, and the associated effects the water chemistry is expected to have on system optimization.

Finally, an economic assessment of the Mg-electrode-driven system is important to consider in the context of overall added cost to a wastewater treatment plant and in comparison, to other similar processes. In particular, it is useful to compare to other electrocoagulation technologies that target coagulation and precipitation of target water components. These target water components include heavy metals, hardness, silica, phosphate, organics (measured as chemical oxygen demand, COD or total organic carbon, TOC), and turbidity (Abdel-Shafy et al., 2020; Brahmi et al., 2019; Espinoza-Quiñones et al., 2009; Kobya

and Demirbas, 2015; Rodriguez et al., 2007). A few studies have evaluated the operating costs for treating wastewater using electrochemical methods with sacrificial anodes consisting of Mg (Abdel-Shafy et al., 2020; Hug and Udert, 2013). However, a larger number of studies have examined electrocoagulation systems based on aluminum (Al) (Bayramoglu et al., 2007; Brahmi et al., 2019; Kobya and Demirbas, 2015; Kobya et al., 2016; Lin et al., 2005; Rodriguez et al., 2007) and iron (Fe) (Bayramoglu et al., 2007; Espinoza-Quiñones et al., 2009; Inan and Alaydın, 2014; Kobya et al., 2016). Estimated costs range from 0.25 \$. m<sup>-3</sup> to 1.85 \$.m<sup>-3</sup> (Abdel-Shafy et al., 2020; Bayramoglu et al., 2007; Espinoza-Quiñones et al., 2009; Kobya et al., 2016). A primary difference here in Mg-driven versus Fe- or Al-driven electrocoagulation systems is the treatment goal of nutrient recovery versus the treatment goal of contaminant removal. Most economic assessments found in the literature are based upon theoretical metal anode consumption estimates, which are calculated from the measured cell voltage and current as a function of time. Both Hug and Udert (2013) and Brahmi et al. (2019), however, have demonstrated that experimentally-determined metal (i.e., Mg, Al) consumption can be larger than the theoretical estimate, suggesting that cost analyses based upon theoretical consumption likely underestimate the treatment cost.

In this work, a scaled-up electrochemical batch reactor was constructed to evaluate nutrient removal from natural wastewater sources, with quantification of the kinetics, removal efficiency, water composition, and energy demand of the reactor when a sacrificial magnesium anode and a stainless-steel cathode are used. We also investigated the electrochemical behavior of the pure Mg anode in these complex, nutrient-rich matrixes, including industrial and municipal wastewater sources, by cyclic voltammetry (CV), linear sweep voltammetry (LSV), and electrochemical impedance spectroscopy (EIS) experiments, where the subsequent impact of anodic dissolution on the wastewater composition and quality was assessed. The structure, morphology, and composition of the obtained precipitates on the anode surface were further analyzed by X-ray diffraction (XRD), energy-dispersive X-ray spectroscopy (EDX), and scanning electron microscopy (SEM).

#### 2. Materials and methods

# 2.1. Materials and instrumentation

The electrolysis experiments for nutrient removal from the various wastewater compositions were carried out by applying a 31.9 V cell voltage for 30 min in a scaled-up single-compartment reactor filled with 16 L of the test solution with the distance between the magnesium (Mg, 99.9% pure, 20  $\times$  30  $\times$  0.3 cm, Goodfellow, USA) anode and the 316 stainless steel (316SS,  $20 \times 30 \times 0.3$  cm, Goodfellow, USA) cathode plates held constant at 5 cm, while the solution was continuously stirred at ~15 rpm (S312-60 Mixer, China). The anode and cathode active surface areas were ~980 cm<sup>2</sup>, and the surface-area-to-volume ratio (SA/ V) was 0.061 cm<sup>-1</sup>. The bulk pH and temperature of the test solutions were monitored with a digital research grade benchtop pH/mV meter coupled with a thermometer (HI5221, Hanna Instruments, USA). The experimental electricity usage and energy input were determined by using a Kill-A-Watt monitor (P3 International P4400-VP Monitor). The experimental current was measured and recorded. The experimental setup is shown in Fig. 1a.

The electrochemical and corrosion studies were carried out in a conventional three-electrode cell (Pine Research, USA) connected to a G3000–30,111 potentiostat/galvanostat (Gamry Instruments Inc., USA) equipped with a Gamry Framework data acquisition software (version 7.8.1), where the pure Mg disk (99.9% pure,  $\phi=5$  mm, Goodfellow, USA), a Ag/AgCl (3.0 M NaCl, BASi, USA) and a graphite rod ( $L_{\rm immersed}=2.3$  cm,  $\phi=0.7$  cm, Pine Research, USA) served as the working electrode (WE), the reference electrode (RE) and the counter electrode (CE), respectively, see Fig. 1b. All potentials in this study are referenced against the reference hydrogen electrode (RHE) and were calculated

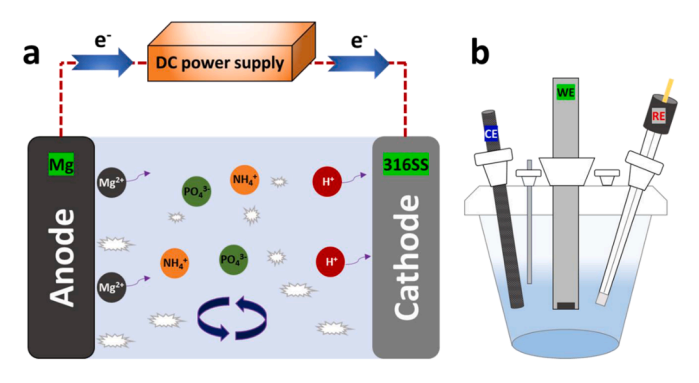


**Fig. 1.** (a) The experimental setup of the scaled-up single-cell electrochemical (2-electrode setup) batch reactor used for the removal of valuable nutrients like phosphorus and nitrogen in wastewaters, and (b) the conventional three-electrode cell setup used for the corrosion studies.

according to equation:

$$E_{\text{RHE}} = E_{\text{Ag/AgCl}} + 0.059 \ pH + E_{\text{Ag/AgCl}}^{\emptyset} \tag{1}$$

where  $E^{\odot}_{Ag/AgCl} = +0.210$  V vs. SHE (298.15 K) and  $E_{Ag/AgCl}$  is the measured working electrode potential. Cyclic voltammograms (CVs) and linear sweep voltammograms (LSVs) were recorded for the various test solutions. Electrochemical impedance spectroscopy (EIS) was performed by applying a 10-mA current, with an AC amplitude of +10 mV vs.  $E_{OCP}$ , over a frequency range of  $0.1-10^6$  Hz. The pH of the bulk test solution was determined before and after the experiments by using a digital pH meter (Orion Star A111, Thermo Scientific). Unless otherwise stated, all electrochemical experiments were performed at room temperature (rt).

# 2.2. Natural wastewater pretreatment

Several types of natural wastewater compositions were obtained: natural poultry wastewater (P-WW, Tyson/River Valley Ingredients, Scranton, AR, USA) and municipal wastewaters from various treatment facilities (F-WW, West Side, Fayetteville, AR; FS-WW, P-Street, Fort Smith, AR, USA; B-WW, Massard, Barling, AR, USA). The raw P-WW was collected before the anaerobic lagoon and contained hot boiler condensate, scrubber/cooling tower bleeds and cooked process water, while the municipal wastewater samples were collected from the influent at the entry point of their respective wastewater treatment plants. The raw wastewater samples were pretreated as described before in our previous papers to remove the colloidal particles and suspended solids (Kékedy-Nagy et al., 2020a). Filtration of the samples was achieved by using a crossflow membrane filtration system with a tubular stainless-steel ultrafiltration membrane (SCEPTER 0.75-250UF-2P, 0.02 µm pore size, Graver Technologies, New Castle County, DE, USA), where the active membrane length was 61 cm (24 inches) with an inside diameter of 0.61 cm (0.24 inches). A Hydra-cell pump (Wanner Engineering, Minneapolis, MN, USA) was used to maintain a flow rate of 7.9 L.min<sup>-1</sup> (2.1 gal.min<sup>-1</sup>, a flow velocity of 15 fps). The unit was operated at 35 psi pressure, and the feed temperature was limited to 25 °C by a circulating water bath (MultiTemp® III, Pharmacia Biotech). The pretreated wastewaters were collected from the permeate side for the electrochemical experiments, and their compositions are shown in Table S1.

# 2.3. Surface and material characterization

The elemental compositions and morphologies of the produced precipitates on the electrode surface were evaluated using a scanning electron microscope (SEM, FEI Nova Nanolab 200 Dual-Beam). The SEM images were further processed by using NIH ImageJ, an open-source

image-processing program. The crystal structure analysis was performed on a Philips PW1830 double system diffractometer, equipped with a Cu cathode. For characterization purposes, the thin deposited film was gently collected from the anode surface to eliminate any possible interference from the Mg substrate on the resulting spectra. Before and after the electrochemical studies, the composition and the characteristics of the wastewater samples were determined by the Arkansas Water Resource Center Water Quality Laboratory (AWRC-WOL).

# 2.4. Experimental calculations

The total hardness expressed as equivalent of calcium carbonate  $(CaCO_3)$  was determined using the following equation (Martínez et al., 2010):

$$TH[CaCO_3] = 2.497x[Ca^{2+}] + 4.118x[Mg^{2+}]$$
 (2)

where *TH* is the total hardness as CaCO<sub>3</sub> (mg.L<sup>-1</sup>), [Ca<sup>2+</sup>] is the calcium ion concentration, and [Mg<sup>2+</sup>] is the magnesium ion concentration, both expressed in mg.L<sup>-1</sup>. The phosphate removal efficiency after the electrochemical experiments in the various wastewater compositions were calculated using the following equation (Lin et al., 2018):

$$PO_{4\text{Rem}}^{3-} = \frac{(C_0 - C_t)}{C_0} \times 100\%$$
 (3)

where  $PO_4^{3-}_{Rem}$  is the phosphate removal efficiency (%),  $C_0$  is the initial (t=0) phosphate concentration (mg.L<sup>-1</sup>), and  $C_t$  is the phosphate concentration at time t (mg.L<sup>-1</sup>).

The ammonium removal efficiency was calculated by using the same approach as described for  $PO_4^{3-}_{Rem}$  in Eq. (3):

$$NH_{4Rem}^{+} = \frac{\left(C_o^* - C_f^*\right)}{C_o^*} \times 100\%$$
 (4)

where  $\mathrm{NH_4}^+_\mathrm{Rem}$  is the ammonium removal efficiency (%),  $C_0^*$  is the initial (t=0) ammonium concentration (mg.L<sup>-1</sup>), and  $C_\mathrm{f}^*$  is the final ammonium concentration (mg.L<sup>-1</sup>).

The rate constant (k) values for phosphate ( $PO_4^{3-}$ ) removal were obtained from the slopes of the zero-order reactions in various concentrations of natural industrial- and municipal wastewater compositions, where two distinct time regions: (i) 0- and 1-min, and (ii) 1- and 30-min, were observed. The k values are reported for time region (ii) only, as k values for (i) could not be calculated due to a lack of additional time points.

The corrosion current was obtained using the Stern-Geary equation:

$$I_{corr} = \frac{\beta_a \times \beta_c}{2.303 \times R_p \times (\beta_a + \beta_c)}$$
 (5)

where  $I_{\rm corr}$  is the corrosion current (A),  $\beta_{\rm a}$  and  $\beta_{\rm c}$  are the anodic and cathodic Tafel slopes (V.dec<sup>-1</sup>), respectively,  $R_{\rm p}$  is the polarization resistance ( $\Omega$ ).

The corrosion rate was estimated according to the following equa-

$$v_{corr} = \frac{I_{corr} \times K \times EW}{\rho \times A}$$
 (6)

where  $v_{\rm corr}$  is the corrosion rate in millimeter per year (mm.y<sup>-1</sup>), K is a constant that defines the units of the corrosion rate (K=0.0254), EW is the equivalent weight (g.eq<sup>-1</sup>),  $\rho$  is the density (g.cm<sup>-3</sup>) [for pure Mg,  $\rho=1.74$  g.cm<sup>-3</sup>], and A is the geometrical area of the disk electrode (A=0.196 cm<sup>2</sup>).

#### 2.5. Operating costs and economic evaluation

When considering the cost of EC treatment, two parameters are generally evaluated as primary cost items, the electrode material and energy costs (Kobya et al., 2016). In this study, the operational costs of the electrochemical process, reported as  $\$.m^{-3}$  of treated wastewater were calculated both experimentally and theoretically. Theoretical calculation is the most commonly used method for estimating input consumption and comparing operational costs in EC studies. Here, we have obtained theoretical values for operating costs by using the following parameters and formulas as referenced in previous literature (Abdel-Shafy et al., 2020; Brahmi et al., 2019):

Operating 
$$cost = aC_{energy} + bC_{electrode}$$
 (7)

where a is the industrial energy price: 0.07 (\$ kW.h<sup>-1</sup>); b is the magnesium cost: 5.51 (\$.kg<sup>-1</sup>);  $C_{energy}$  is electrical energy consumption (kWh.m<sup>-3</sup>), and  $C_{electrode}$  is Mg anode consumption (kg.m<sup>-3</sup>). The unit prices for a and b are averages from the US market in 2021 and 2020, respectively (US EIA, 2021; USGS, 2021).

Theoretical energy consumption was calculated using the following formula:

$$Cenergy = \frac{Uc \times I \times t}{V} \tag{8}$$

where  $C_{\text{energy}}$  is the theoretical energy consumption (kWh.m<sup>-3</sup>),  $U_c$  is the cell voltage (V), I is the average measured current (A), t is the time of electrolysis (h) and V is the volume of wastewater treated (m<sup>3</sup>).

Electrode consumption was theoretically determined by the following equation according to Faraday's Law:

$$Celectrode = \frac{I \times t \times M}{n \times F \times V}$$
 (9)

where  $C_{\rm electrode}$  is the theoretically determined electrode consumption (kg.m<sup>-3</sup>), I is the current (A), t is the time of electrolysis (s), M is molecular mass of magnesium (24.31 g.mol<sup>-1</sup>), n is the number of electrons transferred (n = 2), F is Faraday's constant (96,487 C.mol<sup>-1</sup>) and V is volume of wastewater treated (m<sup>3</sup>).

The experimental energy consumption was measured for the 2-electrode setup using a Kill-A-Watt monitor. The experimental Mg consumption was determined by calculating the total Mg measured in the treated wastewater solution plus the amount of Mg consumed as a result of phosphate precipitation. We note that the experimental Mg consumption is an estimate based upon the assumption that all of the phosphate precipitated as struvite. It is likely that the experimental Mg consumption is an underestimate as results described below suggest that there was also precipitation of magnesium hydroxide species. Further detailed studies would be necessary to delineate precipitate species.

The current efficiency (*CE*) was calculated by dividing the dissolved Mg ( $m_{\rm Mg,\ dissolved}$ ) by the value expected from the measured current ( $m_{\rm Mg,\ current}$ ) using the following equation:

$$CE = \frac{m_{\rm Mg,dissolved}}{m_{\rm Mg,current}} \times 100\% \tag{10}$$

where CE is the current efficiency (%),  $m_{\rm Mg, dissolved}$  is the mass of the Mg dissolved in solution and precipitate (g), and  $m_{\rm Mg, current}$  is the expected Mg dissolved according to the current (g).

The dissolved mass of Mg ( $m_{\rm Mg,dissolved}$ ) was determined by inductively coupled plasma-atomic emission spectroscopy (ICP-AES, Method 200.7), while the expected Mg release based upon the measured current ( $m_{\rm Mg,current}$ ) was evaluated according to Faraday's law of electrolysis by using the following equation:

$$m_{\rm Mg, \ current} = \frac{M_{\rm Mg}Q}{zF} \tag{11}$$

where z is the magnesium valence (2), F is the Faraday constant (96,485.3329 C.mol<sup>-1</sup>),  $M_{\rm Mg}$  is the molar mass of Mg (24.3 g.mol<sup>-1</sup>), and Q is the electric charge (C) obtained from the integration of the I vs. t curve (where I is current in A and t is time in s).

# 3. Results and discussion

#### 3.1. Nutrient removal and water chemistry of natural wastewaters

First, the practicality of nutrient removal from various natural wastewater sources (see Section 2.2) using the scaled-up electrochemical batch reactor was investigated. The reactor's performance along with the bulk pH and total hardness (TH) of the respective wastewater effluent measured prior and after the electrochemical experiments are presented in Table 1. The energy input for nutrient removal varied between 0.63-1.25 kWh.m<sup>-3</sup> and depended upon the wastewater source. All compositions exhibited an increase in their respective pH values, where the F-WW had the highest, with a 2.0-unit increase. This was followed by the FS-WW and B-WW with a 1.5-1.2-unit increase, respectively, while the P-WW showed only a 0.4-unit increase in the pH. Based upon the main electrochemical reactions (see Supporting information). the pH increase of the wastewater effluents promotes the hydrogen evolution reaction (HER) which occurs simultaneously along with the Mg<sup>2+</sup> release. Based upon the TH as expressed in Eq. (2), the P-WW (16.9 mg,L<sup>-1</sup> CaCO<sub>3</sub>) was classified as soft water, the FS-WW (48.9 mg.L<sup>-1</sup> CaCO<sub>3</sub>) and B-WW (56.8 mg.L<sup>-1</sup> CaCO<sub>3</sub>) were both classified as slightly hard waters, while the F-WW (122.4 mg.L<sup>-1</sup> CaCO<sub>3</sub>) was classified as hard water (Table 1; see Table S1 for Ca<sup>2+</sup> and Mg<sup>2+</sup> concentrations). During the electrochemical experiments, a significant increase in the TH was observed in all the wastewater samples, which placed all of them in the hard water classification. This increase was caused by release of Mg<sup>2+</sup> from the Mg anode, along with no measurable Ca<sup>2+</sup> loss through precipitation (Table S2). This progressive change of the TH over time could have a negative impact on the water quality and influence nutrient removal through electrochemical precipitation.

Based upon the complexity of the wastewater effluents, multiple water components present (Table S1) are expected to play a role in nutrient precipitation and phosphate removal kinetics (Table 1). Therefore, it is likely that multiple wastewater components contributed to the enhanced phosphate removal observed for P-WW (Fig. 2). The presence of Cl- and NH<sub>4</sub>+ together enhances Mg anode corrosion (Abbasi et al., 2017; Curioni et al., 2016; Ge et al., 2021; Williams and Neil McMurray, 2008) and therefore enhances struvite precipitation due to the increased availability of Mg<sup>2+</sup> in solution. Across the four wastewaters tested, P-WW has the highest combined concentration of Cl<sup>-</sup> and NH<sub>4</sub><sup>+</sup>, a finding which is in good agreement with the enhanced phosphate removal kinetics observed for P-WW (Table 1 and Fig. 2). The pH of the bulk solution and near the Mg electrode also plays a role, as increasing pH enhances Mg(OH)2 formation as a passivating film and as a precipitate; pH changes ion speciation and therefore change water chemistry effects on both Mg corrosion and precipitation. In particular, the higher initial pH of the F-WW sample likely reduced Mg corrosion by reducing NH<sub>4</sub><sup>+</sup> speciation and causing enhanced passivation at the Mg anode surface.

In contrast to the effects of Cl $^-$  and NH $_4^+$ , the presence of Ca $^{2+}$  may have a negative impact on nutrient precipitation and phosphate removal. Generally, the presence of significant Ca $^{2+}$  concentrations (i.e., ratios of Ca:Mg  $\geq 1.0$ ) may enhance the precipitation of Ca $^{2+}$ -PO $_4^{3-}$  solids, therefore further reducing the purity of the electrochemically obtained struvite. One way to reduce the interference of Ca $^{2+}$  is by adding extra chemicals to chelate the Ca $^{2+}$  ions or fix the pH (Shen et al., 2010; Zhou et al., 2015), however this may lead to an increase in the operating costs and might change the stoichiometry of the wastewater composition. In an alternative approach, in this study, we applied a limited electrolysis time (i.e., 30 min) to minimize the precipitation of calcium in the form of hydroxyapatite or amorphous calcium phosphate

**Table 1**The initial pH (pH<sub>i</sub>); final pH (pH<sub>f</sub>); initial total hardness ( $TH_i$ ); final total hardness ( $TH_f$ ); energy consumption; phosphate removal efficiency (PO<sub>4</sub><sup>3-</sup><sub>Rem</sub>,%); ammonium removal efficiency (NH<sub>4</sub><sup>+</sup><sub>Rem</sub>,%); and phosphate removal rate constant (k).

| Samples | $pH_{\rm i}$ | $pH_{\rm f}$ | $\mathrm{TH_{i}}^{a}$ (mg.L $^{-1}$ ) | $\mathrm{TH_{f}}^{a}$ (mg.L $^{-1}$ ) | Energy consumption (kWh.m <sup>-3</sup> ) | PO <sub>4</sub> <sup>3-</sup> <sub>Rem</sub> <sup>b</sup> (%) | $\mathrm{NH_4}^+_{\mathrm{Rem}}^{\mathrm{c}}$ (%) | $k^{\mathrm{d}}(\mu\mathrm{M.min}^{-1})$ |
|---------|--------------|--------------|---------------------------------------|---------------------------------------|---|---|---|--|
| P-WW    | 8.6          | 9.3          | 16.9                                  | 151.8                                 | 1.25                                      | 93.0  | 12.5  | 0.622                                    |
| F-WW    | 10.2         | 12.1         | 122.4                                 | 169.6                                 | 0.63                                      | 47.5  | 18.9  | 0.245                                    |
| FS-WW   | 8.5          | 9.7          | 48.9                                  | 167.3                                 | 0.63                                      | 44.4  | 14.3  | 0.472                                    |
| B-WW    | 7.9          | 10.4         | 56.8                                  | 224.2                                 | 0.63                                      | 44.6  | 12.3  | 0.294                                    |

initial total hardness according to Eq. (2).

d phosphate removal rate constant for zero-order kinetics between t = 1 min and t = 30 min.

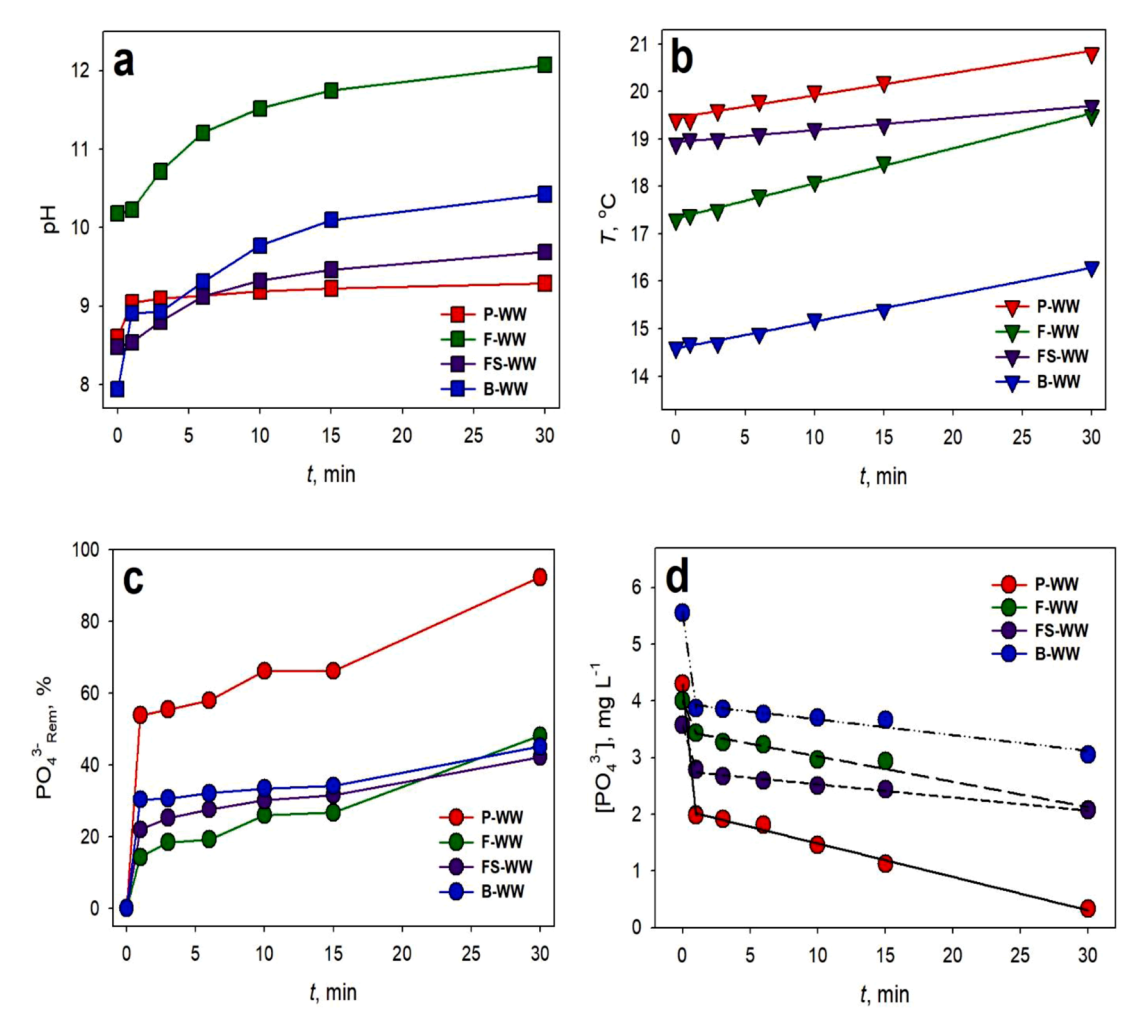


Fig. 2. The evolution of (a) pH, (b) temperature of the bulk solution, (c) phosphate removal efficiency (PO<sub>4</sub><sup>3-</sup><sub>Rem</sub>,%), and (d) PO<sub>4</sub><sup>3-</sup> concentration over time in the various natural wastewater compositions during electrochemical nutrient removal.

due to slower reported Ca precipitation kinetics (Lahav et al., 2013).

The presence of Ca<sup>2+</sup> ions has been shown to slow the kinetics of struvite precipitation by lengthening the induction time to nucleation (Acelas et al., 2015; Kabdaszli et al., 2006; Le Corre et al., 2005; Yan and Shih, 2016). The work by Li et al. showed that lower concentrations of Ca<sup>2+</sup> and/or lower Ca:Mg molar ratios minimize the impact of Ca on struvite precipitation kinetics (Li et al., 2016), suggesting there may be a minimum Ca<sup>2+</sup> concentration/ratio threshold for observation of slowed kinetics. This threshold requirement is likely a contributing factor in our results, where P-WW had a larger rate constant for phosphate removal, as compared to the other three wastewater samples, even though the [Ca<sup>2+</sup>] varied amongst F-WW, FS-WW, and B-WW. It is also possible that the larger organic carbon content of the P-WW wastewater contributed

to Ca<sup>2+</sup> complexation, which may have reduced the negative effects of Ca on nutrient precipitation in the P-WW sample (Rabinovich and Rouff, 2021).

The natural wastewater samples tested contained in general between 3.6–5.6 mg.L $^{-1}$  of  $\mathrm{PO_4}^{3-}$ , while the concentration of  $\mathrm{NH_4}^+$  was higher at 15–32 mg.L $^{-1}$  (see Table S1), which makes, in this case, the  $\mathrm{PO_4}^{3-}$  the limiting component of the electrochemically precipitated struvite. The scaled-up batch reactor achieved a remarkable  $\mathrm{PO_4}^{3-}$  removal efficiency of 92.3% from the P-WW and between 42.2–48.1% from the municipal wastewater samples, while the  $\mathrm{NH_4}^+$  removal efficiency was apparently smaller and varied between 12.3–48.9%, see Table 1. This apparent discrepancy is explained by the initial concentration difference observed for the  $\mathrm{NH_4}^+$  which was 4 to 8 times higher than the  $\mathrm{PO_4}^{3-}$ , depending

b phosphate removal efficiency according to Eq. (3).

c ammonium removal efficiency according to Eq. (4).

on the wastewater sample. However, based upon their absolute concentration decrease (see Table S2), the  $\mathrm{NH_4}^+$ : $\mathrm{PO_4}^{3-}$  showed a 1:1 removal ratio in most of the wastewater samples tested, which is in good agreement with the stoichiometric ratio of struvite.

The mechanism of electrochemical ammonia removal from wastewater is complicated, as it is affected by the electrode material, and electrolyte ionic species present in the wastewater matrix (Yao et al., 2016). In addition to precipitation reactions (e.g., struvite formation), ammonia can also be removed through oxidative reactions. Ammonia speciation sits between the molecular and ionic forms, where the alkaline pH favors the presence of the molecular form (NH3), while neutral and acidic pH favor the presence of the ionic form (NH<sub>4</sub><sup>+</sup>). Based upon the solution pH, ammonia can be removed via direct electrooxidation through direct electron transfer (pH > 9) or indirect oxidation by an oxidation mediator such as Cl<sub>2</sub>, HOCl or OCl<sup>-</sup> (pH < 7) produced on the anode surface (Zöllig et al., 2015). Moreover, the removal efficiency is affected by the temperature, applied current density, and the Cl<sup>-</sup> concentration. For reaction kinetics, a pseudo first-order rate was reported (Szpyrkowicz et al., 1995), whereas others proposed a pseudo zero-kinetics due to the regeneration of Cl<sup>-</sup> during electrolysis (Vanlangendonck et al., 2005). For example, Kim et al. found faster degradation of ammonia, which was achieved using electro-oxidation process in chlorinated aqueous solution under alkaline conditions (Kim et al., 2006).

Based upon the high pH<sub>i</sub> (see Table 1) of the F-WW sample, ammonia removal may have occurred based upon direct electron transfer with minimal by-product formation, while for P-WW and FS-WW samples, the indirect oxidation via active chlorine was likely to be the main mechanism for ammonia removal. It might be expected that if ammonia is being oxidized, there would be halogenated by-products present in the wastewater composition after electrolysis. On the other hand, electrochemical ammonia removal in the B-WW sample would proceed through an indirect oxidation by active radicals at the start (pH $_{\rm i}$  ~7.9) which could potentially turn into direct electro-oxidation (pH  $_{\rm f}$   $\sim$ 10.4) towards the end. Moreover, based upon the main electrochemical reactions (see Supporting information), the localized pH increase near the anode/cathode would further produce a shift of ammonium ions to ammonia, resulting in nitrogen losses due to ammonia volatilization. However, it is not possible to completely delineate the ammonia removal mechanisms, and this aspect of understanding how the wastewater composition changes with Mg driven electrochemical treatment warrants further investigation in future studies.

Intrigued by the initial results, we further studied the evolution of pH, temperature of the bulk solution, PO<sub>4</sub><sup>3-</sup> removal efficiency, and PO<sub>4</sub><sup>3-</sup> concentration change over time, in the various natural wastewater samples during electrochemical nutrient removal (Fig. 2). As expected, the pH showed an increasing trend over time, where the largest change was observed at the start of the experiments, then reaching a plateau at 15 min in the case of the municipal wastewater samples. The pH in the industrial wastewater sample (P-WW) reached a plateau after 1 min (Fig. 2a). The temperature showed a steady linear increase over time for all the samples (Fig. 2b). The greatest PO<sub>4</sub><sup>3-</sup> removal occurred within 1 min of electrolysis, i.e., 54% in P-WW and 14-30% in the municipal wastewater samples (Fig. 2c). The pH of the test solution is considered to be a key factor in the PO<sub>4</sub><sup>3-</sup> removal, as a result of the  $\mathrm{PO_4}^{3-}$  ions speciation, where in alkaline solutions the  $\mathrm{PO_4}^{3-}$  (HPO $_4^{2-}$ /  $PO_4^{3-}$   $pK_a$  is ~12.67) form dominates (Krężel and Bal, 2004; Stoll and Blanchard, 1990; Yan et al., 2004). On the other hand, in complex matrices such as raw industrial or municipal wastewater sources, besides the solution pH, other interfering elements may influence the PO<sub>4</sub><sup>3-</sup> removal to a greater extent.

The  $PO_4^{3-}$  concentrations versus time during the electrochemical nutrient removal in the various natural wastewater compositions are presented in Fig. 2d. Two kinetic regions are evident, where fast removal occurs within 1 min, and the kinetic relationship for phosphate removal shifts after that time. It can also be observed that the  $PO_4^{3-}$ 

concentration displays a linear relationship with time between 1 and 30 min, suggesting that the reaction follows a zero-order kinetic rate law in this region. The  ${\rm PO_4}^{3-}$  removal rate constants (k) were obtained for the second kinetic region from the slope and are presented in Table 1, where the k values for P-WW were 1.3–2.5 units higher than those obtained for the municipal wastewaters. Based upon the slope of the first kinetic region, i.e., between 0 and 1 min, the reaction kinetics are expected to be significantly faster in this initial time frame and could be dependent upon the reactant concentrations.

The significant decrease in the PO<sub>4</sub><sup>3-</sup> removal kinetics after 1 min could be attributed to the: (i) formation of a Mg(OH)2 passivating layer and (ii) bubble formation on the anode surface. The formation of the precipitates act as an insulating layer which has an adverse effect on the anode performance (i.e., decreased Mg corrosion and decreased nutrient recovery), which has been reviewed intensively over the years (Hug and Udert, 2013; Kékedy-Nagy et al., 2019, 2020b; Kruk et al., 2014). Normally, precipitates cover the Mg anode surface forming a passivating layer, which act as a second cathode to accelerate Mg<sup>2+</sup> release at first. However, at some point, the passivating layer may reduce the ability of the sacrificial anode to corrode and release Mg<sup>2+</sup>. Although not captured, due to safety reasons, during the electrochemical nutrient removal experiments, significant bubble formation on the anode surface was visually confirmed, indicating possible molecular hydrogen, H2 formation. Based upon the major chemical reactions (see Supporting information), it is expected that alongside nutrient removal, H2 production should occur on the anode and cathode surfaces, respectively. It is expected that the H<sub>2</sub> bubbles would further block the Mg active sites on the anode surface, therefore, slowing down the PO<sub>4</sub><sup>3-</sup> removal kinetics after

On the other hand, the significant difference in the PO<sub>4</sub><sup>3-</sup> removal efficiency over time and k observed between the P-WW and municipal wastewater samples can be attributed to multiple components and their combined effects, as described above. In particular, the presence of Cl and NH<sub>4</sub><sup>+</sup> species in P-WW disrupt the passivating oxide, enabling higher Mg corrosion rates, and the presence of higher organic carbon content enables Ca<sup>2+</sup> complexation and reduces the effect of Ca on struvite precipitation. The higher levels of Ca<sup>2+</sup>, contributing to the *TH* as expressed in Eq. (2), in the other three wastewater samples likely delayed struvite nucleation and precipitation. Overall, these different components would have a combined effect in P-WW to cause an enhancement in the kinetics of phosphate removal. In recent work, Ge et al. showed that the presence of NH<sub>4</sub><sup>+</sup> enhanced Mg corrosion in the presence of Cl<sup>-</sup>, while Cai et al. elegantly showed during electrochemical nutrient removal, the surface of the Mg was first oxidized to MgO which transformed into Mg(OH)2, MgNH4PO4, and MgCO3. (Cai et al., 2021; Ge et al., 2021).

Next, we studied the overall composition of the wastewater samples before and after the electrochemical experiments using the scaled-up batch reactor in more detail, see Tables S1, S2. It can be observed that the concentrations of the PO<sub>4</sub><sup>3-</sup> and the NH<sub>4</sub><sup>+</sup> decreased, which was associated with the formation of the precipitates observed on the surface of the pure Mg anode during the electrochemical nutrient removal experiments. The concentration of the major anions and cations present in the wastewater samples before and after the experiments are summarized in Fig. 3. It can be observed that the  $K^+$ , Na<sup>+</sup>, SO<sub>4</sub><sup>2-</sup>, Cl<sup>-</sup>, and NO<sub>3</sub><sup>-</sup> ionic species showed a decrease in their concentrations, which could potentially improve the water quality of the effluents. On the other hand, Ca<sup>2+</sup> showed a slight increase, whereas the Mg<sup>2+</sup> ionic species showed a significant increase in their concentrations in all four wastewater samples tested, see Fig. 3. It is expected that the increase in the concentrations of these ionic species would change the conductivity ( $\sigma$ ) of the aqueous solutions, as well as the TH. Based on the results, the general increase in hardness observed in the wastewater samples can be mainly attributed to the Mg<sup>2+</sup>, due to the release of Mg<sup>2+</sup> during anodic corrosion. Moreover, the slight increase in the Ca<sup>2+</sup> concentration in the samples also suggest that little to no Ca<sup>2+</sup> precipitated during the

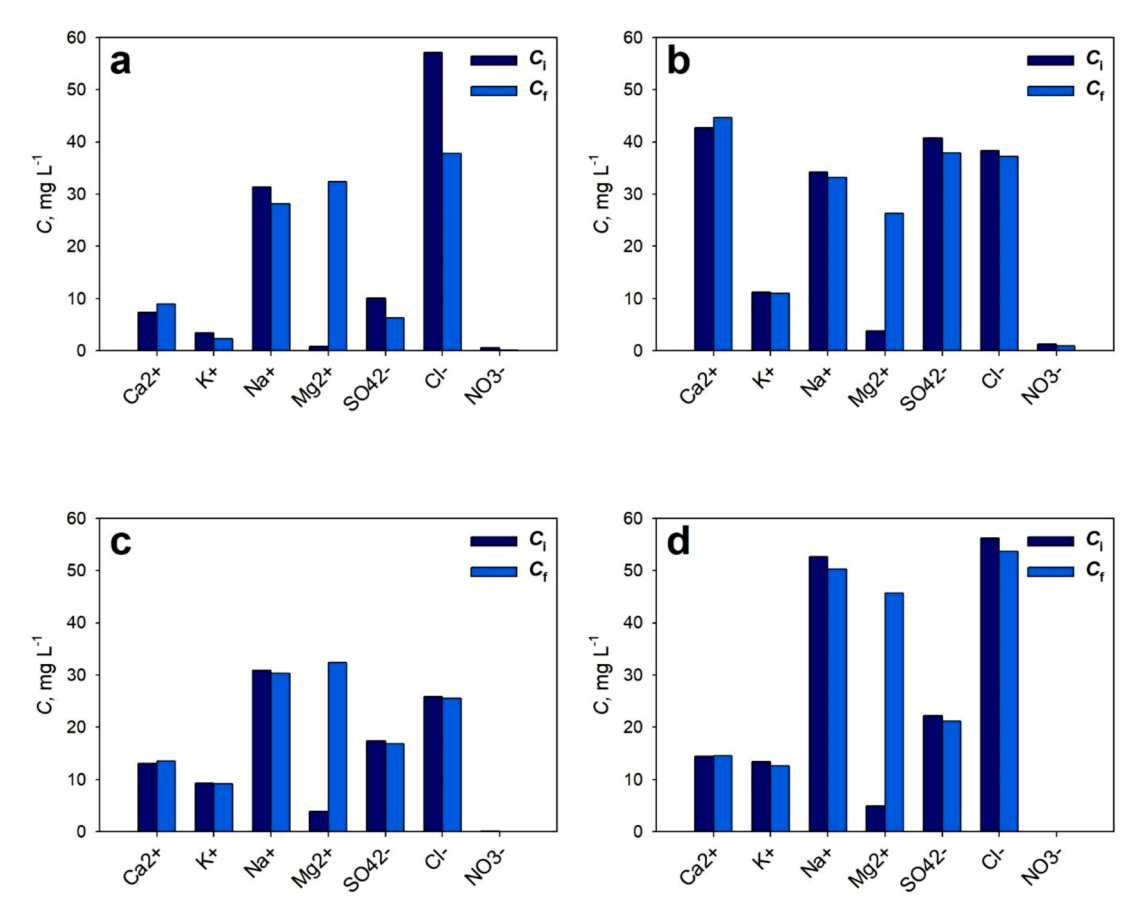


Fig. 3. The concentration of the major anions and cations present before and after the electrochemical nutrient removal using the scaled-up single-cell batch reactor in the various wastewater effluents: (a) P-WW, (b) F-WW, (c) FS-WW, and (d) B-WW.

electrochemical nutrient precipitation process.

The evolution of important water quality parameters such as the conductivity ( $\sigma$ ), total organic carbon (TOC), total dissolved solids (TDS), and total suspended solids (TSS) during the electrochemical nutrient removal experiments are presented in Fig. 4 and Tables S1, S2. The  $\sigma$  showed an increasing trend in all the samples due to the increase in the concentrations of the Ca<sup>2+</sup> and Mg<sup>2+</sup>, see Fig. 3. The most significant change in the  $\sigma$  was observed for the P-WW sample with a 254unit increase, followed by FS-WW (120-unit) and B-WW (116-unit), while the lowest change was observed for the F-WW, with only a 30-unit increase, see Fig. 4a. Interestingly, the  $\sigma$  of the respective wastewater matrix had no major influence on the  $PO_4^{\,3-}$  and  $NH_4^{\,+}$  removal efficiencies, respectively. The TDS showed an increase after the electrochemical experiments as well, see Fig. 4c, which may be explained by the significant increase of the  ${\rm Mg}^{2+}$  ions in the wastewater effluents due to anodic corrosion as shown in Fig. 3. The slight increase of Ca<sup>2+</sup> in the wastewater effluents, see Fig. 3, could also have an effect on the TDS increase. On the other hand, it can be observed that the TOC and TSS showed a decrease in all the wastewater effluents, see Fig. 4b, d, which demonstrates an improvement of water quality. This result suggests that individual water components, rather than the total dissolved solids as a whole, affect the electrochemical precipitation process.

The water quality was impacted by the electrochemical nutrient removal process after which the water quality showed an overall improvement, however not at the level expected. Although, the various wastewater effluents were characterized by a lower amount of  $K^+$ , Na $^+$ , SO<sub>4</sub> $^{2-}$ , Cl $^-$ , and NO<sub>3</sub> $^-$  ionic species, while important water quality indicators such as the TOC and TSS showed a significant removal as well; other parameters such as the  $\sigma$ , Mg<sup>2+</sup>, Ca<sup>2+</sup>, and TDS showed an increase. Most importantly, the biggest concern is the elevated pH<sub>f</sub>, which varied between 9.3 – 12.1 and is considered high to the accepted level of

6.5-8.5 of surface waters; therefore, the treated effluents could not be discharged into receiving water bodies. These results show that the electrochemical nutrient removal process should be implemented in the wastewater treatment plant process flow as a supplementary step, and pH adjustment would be necessary prior to the treated water being discharged.

# 3.2. Electrochemistry and corrosion of pure-Mg in natural wastewaters

Due to the importance of the corrosion and passivation behavior of Mg during electrochemical nutrient removal in complex matrixes such as natural industrial or municipal wastewater sources, we decided to further study Mg electrode behavior by using a conventional threeelectrode cell setup as shown in Fig. 1b. As a first step, we investigated the electrochemical behavior of a pure Mg disk working electrode (WE) by cyclic voltammetry (CV, not IR corrected) in various natural wastewater compositions at a scan rate of 50 mV.s<sup>-1</sup> and rt (Fig. 5). The figure shows that the obtained full CVs are similar, with no major anodic or cathodic peaks observed in the potential window employed, indicating electrode passivation, electrodeposition, or product formation at the electrode surface. Additionally, the increased currents observed in the reverse scans for all the samples would further suggest a dynamic change occurring at the electrode surface during that period (Fig. 5). The Mg passivation region, where essentially zero current is produced, is similar for the three municipal wastewater sources, even though the maximum measured current density varies between the three samples. However, the Mg passivation region for the P-WW sample is shifted to a more negative potential region, as compared to the municipal wastewater sources, suggesting that the water composition facilitated a more energetically favorable Mg corrosion process and associated current response.

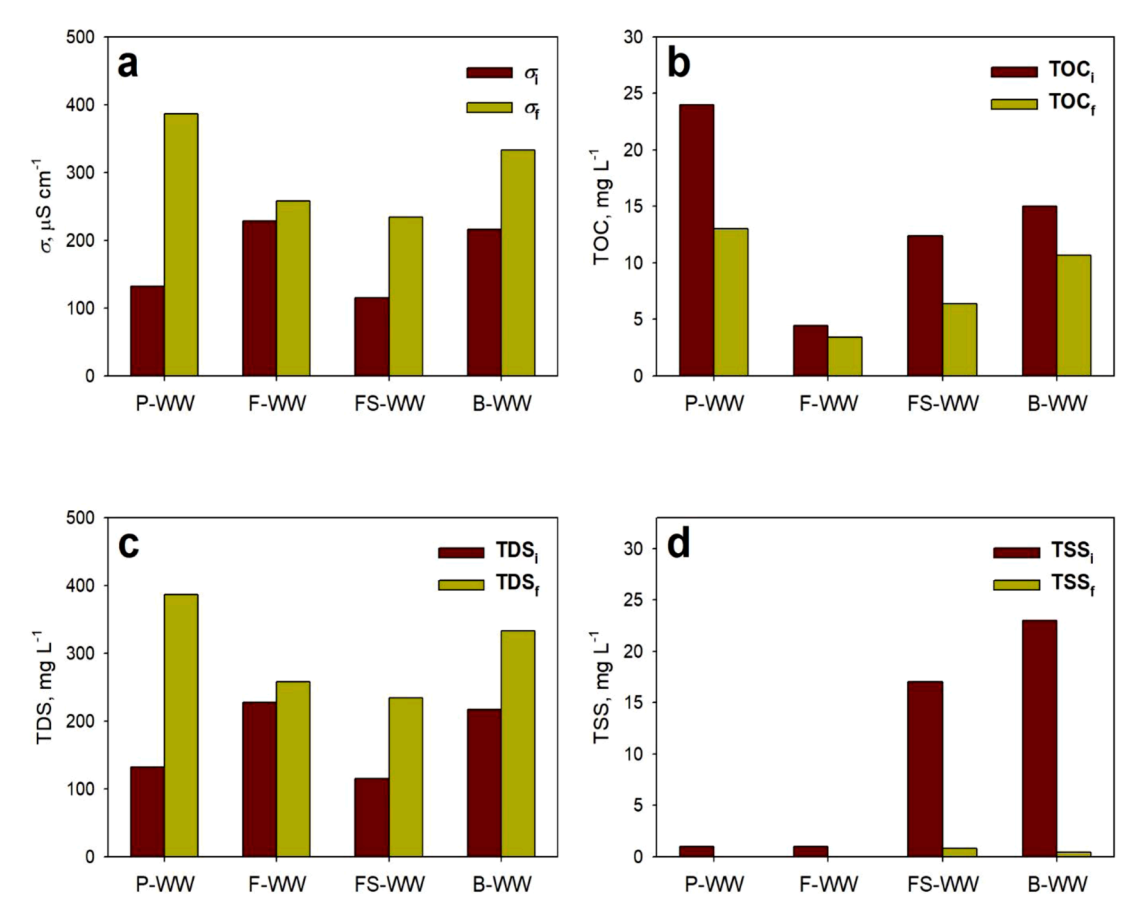


**Fig. 4.** The (a) conductivity ( $\sigma$ ), (b) total organic carbon (TOC), (c) total dissolved solids (TDS), and (d) total suspended solids (TSS) measured before and after the electroless nutrient removal with scaled-up single-cell electrochemical batch reactor in the various wastewater effluents.

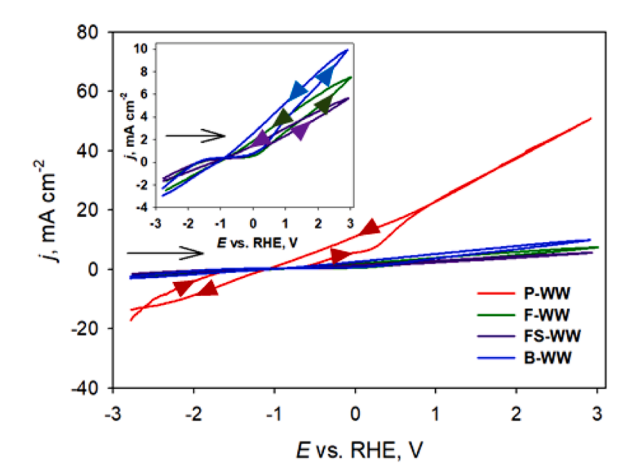
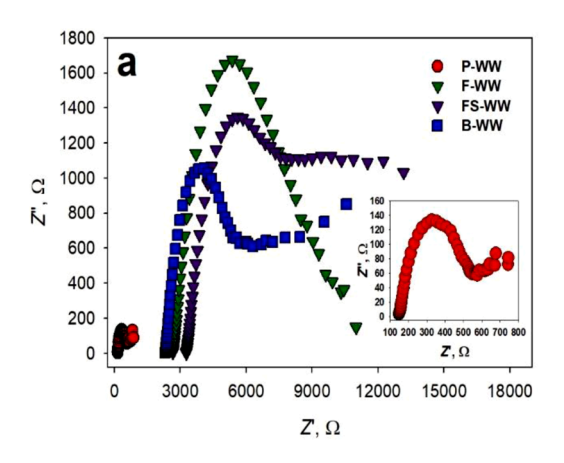


**Fig. 5.** The full cyclic voltammograms (CVs) recorded with the pure Mg disk electrode in various types of wastewaters at rt with a scan rate of 50 mV.s<sup>-1</sup>. Inset: The CVs recorded in municipal wastewater sources.

Next, we studied the electrochemical behavior of the pure Mg discs by electrochemical impedance spectroscopy (EIS) in the various types of wastewaters, where the subsequent Nyquist and Bode plots are presented in Fig. 6. The Nyquist plots, see Fig. 6a, revealed similar capacitance arc shapes or semi-circles in all the samples; however, the semi-circle diameter associated with the polarization resistance ( $R_p$ ) clearly varied with the wastewater composition and showed an increase for the municipal sources, see Table 2. Moreover, it can be observed that the uncompensated resistance ( $R_u$ ), which is associated with the solution

resistance, is significantly higher in the case of the municipal wastewaters, see Table 2. This result appears to be correlated to the higher total hardness and the lower chloride/ammonium concentrations of the municipal wastewaters, as compared to the poultry processing wastewater, as the TDS of the P-WW sample was not high relative to the other wastewater samples (see Table S1). Based upon the obtained  $R_{\rm p}$  values, the pure Mg disk anode showed the lowest corrosion resistance in the P-WW sample; therefore, the pure Mg anode is expected to have a higher corrosion rate in the P-WW sample since the current corrosion is inversely related to the  $R_{\rm p}$  according to the *Stern-Geary* equation, see Eq. (5). This result aligns with our results in Table 1 and Fig. 2, where the P-WW sample results in faster phosphate removal kinetics and larger phosphate removal efficiencies.

It should be noted that it was difficult to model the semi-circles obtained in the Nyquist plots (Fig. 6a) and not possible to fit a circuit to determine the  $R_{\rm p}$  or  $R_{\rm u}$  values accurately; therefore, the reported values shown in Table 2 should be considered relative rather than absolute. The significant variations at low frequencies observed in the municipal wastewater sources are typically indicative of systems containing significant electrolyte resistance and are obtained for systems where the surface of the anode is undergoing dynamic changes (i.e., molecular hydrogen bubble formation or/and solids produced and accumulated on the magnesium surface) (Zhang and Zeng, 2012). The electrochemical systems presented show non-steady state behavior due to changes in electrode properties during the experiment, and this non-steady state behavior has a significant impact on the stochastic contribution to the error structure of the EIS measurements. This bias is usually observed most easily at frequencies that require the longest time for measurement and that violate the Kramers-Kronig relations, while instrumental artefacts tend to appear at high frequencies due to equipment limitations (Agarwal et al., 1995; Orazem, 2004; Shukla et al., 2004).



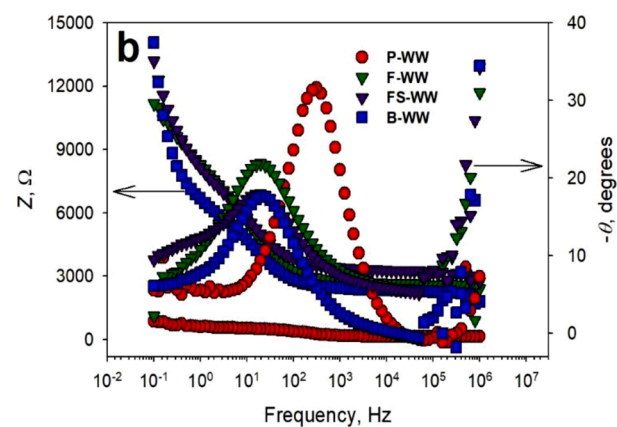


Fig. 6. The EIS data presented in (a) Nyquist plots at the  $E_{OCP}$  (-1.95 V vs. RHE) and (b) Bode plots obtained with the pure Mg disk electrode in various types of natural wastewater sources at rt.

**Table 2**Corrosion data obtained for the pure Mg disk in various natural wastewater sources.

| Wastewater type | $R_u(\Omega)$     | $R_p(\Omega)$     | $E_{\rm corr}({\rm mV~vs.~RHE})$ | $I_{\rm corr}^{\rm a}(\mu {\rm A})$ | $\beta_{\rm c}({\rm mV.dec}^{-1})$ | $\beta_a(\text{mV.dec}^{-1})$ | $v_{\rm corr}^{}({\rm mm.y}^{-1})$ |
|-----------------|-------------------|-------------------|----------------------------------|-------------------------------------|------------------------------------|-------------------------------|------------------------------------|
| P-WW            | 144               | 432               | -1261                            | 135.12                              | 305                                | 390                           | 15.76                              |
| F-WW            | $2.6 \times 10^3$ | $7.4 \times 10^3$ | -959.4                           | 16.29                               | 842                                | 630                           | 1.90                               |
| FS-WW           | $3.0 \times 10^3$ | $9.4 \times 10^3$ | -1163                            | 23.42                               | 871                                | 811                           | 2.73                               |
| B-WW            | $1.9\times10^3$   | $9.7 \times 10^3$ | -1248                            | 29.87                               | 980                                | 656                           | 3.48                               |

<sup>&</sup>lt;sup>a</sup> the corrosion current according to Eq. (5).

To further understand the effect of the various natural wastewater sources on the Mg-based disk electrode material, the potentiodynamic polarization (PDP, not IR corrected) curves were recorded, where the anodic and cathodic branches were generated separately from the corresponding anodic and cathodic LSVs, respectively, with a cleaning step performed in between each LSV. Fig. 7 shows the Tafel plots generated, where it can be observed that there is a well-developed anodic and cathodic branch, respectively; however, neither branch is characterized by a linear Tafel region. At high anodic polarization, the formation of a passivating layer on the pure Mg disk anode in all wastewater sources seemed unavoidable, even though all the samples contained Cl<sup>-</sup> anions in their natural composition (see Table S1), which are expected to have a depassivating effect on the oxide layer. Based upon the polarization curves, the municipal wastewater sources produced a more significant passivation layer which could be explained by the higher TH<sub>i</sub> and lower chloride/ammonium concentrations (see Table 1), while the one recoded in P-WW shifted to a higher current density region which indicates a

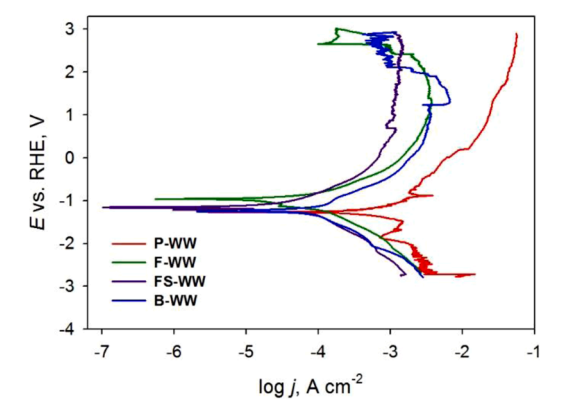


**Fig. 7.** The Tafel plots generated from the LSVs (both branches), recorded with the pure Mg disk electrodes in various types of wastewater sources at a scan rate of 1 mV.s<sup>-1</sup> and at rt.

higher pitting corrosion occurrence, see Fig. 7. This result confirms our previous findings, where the wastewater composition of P-WW, which included not only higher chloride and ammonium ion concentrations but lower calcium concentration and higher organic carbon concentration, appears to have a composition that allows enhanced Mg corrosion and less surface passivation. The variations in the PDB curves at high voltage are due to the formation of bubbles on the surface of the Mg anode, which aligns with our conclusion regarding the influence of both the Mg(OH)<sub>2</sub> passivation layer and the formation of H<sub>2</sub> gas bubbles at the electrode surface contributing to the shift in measured phosphate removal kinetics. The different corrosion parameters such as the corrosion potential ( $E_{\rm corr}$ ), the corrosion current ( $I_{\rm corr}$ ), the anodic ( $\beta_a$ ) or the cathodic ( $\beta_c$ ) Tafel slopes, and the corrosion rate ( $\nu_{\rm corr}$ ) are given in Table 2

The obtained anodic  $(\beta_a)$  and cathodic  $(\beta_c)$  Tafel slopes (see Table 2) show a direct correlation with the natural wastewater composition and origin, where the slopes generally increased when municipal wastewater sources were used. The higher Tafel slopes could be explained by the higher TH<sub>i</sub> and lower organic carbon concentration, [Cl<sup>-</sup>], and [NH<sub>4</sub><sup>+</sup>] observed for the municipal wastewaters (see Table 1), which could have impacted the reaction mechanism(s) and the overall reaction kinetics of nutrient removal. On the other hand, due to the complexity of the natural wastewater matrixes used in this study, it is expected that slight changes in the composition could have a major impact on the overall reaction kinetics and electron transfer process. The pure Mg electrode showed an approx. 5.7-fold increase in the corrosion rate in the P-WW sample compared to the municipal wastewaters. These results are in good agreement with the data obtained from the EIS fitting, where the sacrificial anode showed the lowest corrosion resistance in P-WW compared to the other water samples tested (see Table 2).

# 3.3. Precipitate analysis

The deposits formed on the anode during the nutrient removal experiments conducted with the scaled-up single-cell electrochemical batch reactor in the natural wastewater source was further analyzed

b the corrosion rate in millimeter per year according to Eq. (6).

using various surface characterization techniques (scanning electron microscopy (SEM), X-ray diffraction (XRD), energy-dispersive X-ray spectroscopy (EDX)) to study their structure, morphology, and chemical composition. To eliminate the interfering effects of the Mg substrate on the XRD and EDX spectra, the precipitate was gently removed from the anode surface with a straight razor. The high-resolution SEM image of the precipitate obtained from the P-WW sample is presented in Fig. 8a and it can be observed that showed a different structure from the high-quality struvite obtained in similar conditions in synthetic wastewater composition reported previously by our group (Kékedy-Nagy et al., 2020a, 2019, 2020b).

Interestingly, the elemental mapping, see Fig. 8b, revealed a homogeneous distribution of the significant elements (Mg, O, P and N) usually present in the electrochemically precipitated struvite composition. However, the EDX spectrum (Fig. 8c) displayed two well-defined peaks with their respective atomic percentages (At%) for Mg (24.25 At%) and O (72.06 At%), while the peaks for N (2.54 At%) and P (1.15 At%) were significantly smaller. Finally, the XRD pattern (Fig. 8d) revealed that the precipitate formed on the anode mainly consisted of magnesium hydroxide (Mg(OH)<sub>2</sub>) and showed only a 3% similarity toward the struvite pattern, which is reasonable considering the low P concentrations in the wastewater sources, but also may suggest that the P removal followed an alternative mechanism. One possibility could be through electrocoagulation involving aluminum (Al) and/or iron (Fe). Both metals are present in the Mg anode composition as impurities (N.B. based upon the vendor's specification: Al 70 mg.L<sup>-1</sup>; Fe 280 mg.L<sup>-1</sup>) and could easily be dislodged/dissolved from the anode surface into the wastewater during corrosion. The suspended solids (e.g., gravel, slit, clay, sand, and algae) in the sample might further provide a viable option for P removal, by providing surface area for P adsorption and precipitation. Furthermore, although not determined, microorganisms and bacteria present in the wastewater could provide an alternative pathway for biological P removal as well.

The formation of mainly Mg(OH)2 on the anode surface can be explained by the increased bulk pH of the P-WW sample (Fig. 2a), moreover, an increase in the local pH at the electrode's surface is also expected during the electrolysis, as described previously by Ben Moussa et al. (Ben Moussa et al., 2006), which would further increase the pH and thus negatively impact the struvite formation. In the case of the other wastewater samples, the obtained precipitate was so low that it could not be further analyzed; however, we would not expect a significantly different composition based upon their high pH values measured. Overall, these results show the important role that pH plays in controlling the precipitate(s) that form and suggest that pH control will be necessary for these electrochemical systems to optimally produce struvite as the primary precipitate. Further, the phosphate is the limiting component for struvite precipitation, and due to the higher ammonia concentrations, ammonia is likely to remain even if all of the phosphate is removed through struvite precipitation.

# 3.4. Economic analysis

Current efficiency (*CE*) has been considered in other studies examining *EC* water treatment using Mg (Hug and Udert, 2013) and Al (Brahmi et al., 2019). Similar to previous works (Brahmi et al., 2019; Hug and Udert, 2013), the *CE* was found to be greater than 100% across all treatments (Table 3), where the P-WW sample had the lowest *CE* value of 205% and the B-WW sample showing the largest deviation at 461%. We note that based upon a literature review of calculation methods and a comparison of experimental and theoretical energy consumption data, the primary difference we observe in energy consumption calculations is in the use of experimental versus theoretical Mg consumption data, not in differences between how overall energy consumption is determined. Hug and Udert offer micro-galvanic corrosion

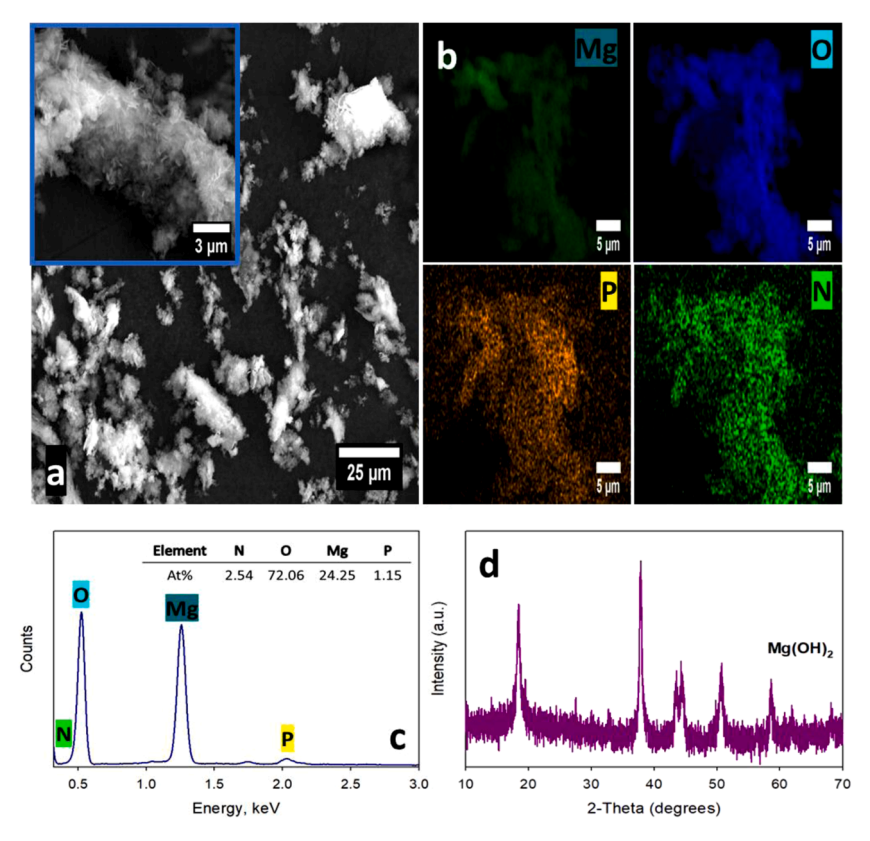


Fig. 8. (a) High-resolution SEM image of multiple precipitate crystals from P-WW electrochemical precipitation. (b) The EDX elemental (Mg, O, P, N) mappings. (c) EDX spectrum with the atomic percentages (At%) of the corresponding elements from the recovered precipitate. (d) Powder XRD patterns of the recovered precipitate.

**Table 3** Summary of the applied cell voltage  $(U_{\rm appl})$  for the 2-electrode system, measured average current  $(I_{\rm ave})$ , theoretical energy consumption, theoretical Mg release  $(m_{\rm Mg,\ current})$ , measured actual Mg release  $(m_{\rm Mg,\ dissolved})$ , current efficiency (CE) as a function of wastewater source.

| Samples | U <sub>appl</sub><br>(V) | I <sub>ave</sub> (A) | Theoretical Energy<br>Consumption <sup>a</sup><br>(kWh.m <sup>-3</sup> ) | m <sub>Mg,</sub> current (g) | m <sub>Mg</sub> , dissolved (g) | <i>CE</i> <sup>d</sup> (%) |
|---------|--------------------------|----------------------|--|------------------------------|---------------------------------|----------------------------|
| P-WW    | 31.9                     | 1.15                 | 1.15   | 0.0163                       | 0.0334                          | 205                        |
| F-WW    | 31.9                     | 0.55                 | 0.548  | 0.0078                       | 0.0268                          | 344                        |
| FS-WW   | 31.9                     | 0.71                 | 0.708  | 0.0101                       | 0.0328                          | 326                        |
| B-WW    | 31.9                     | 0.71                 | 0.708  | 0.0101                       | 0.0463                          | 461                        |

- a calculated from the applied cell voltage and measured average current.
- b the expected Mg release based on the measured current according to Eq. (11).
  - <sup>c</sup> dissolved mass of Mg determined by ICP-AES.
- $^{\rm d}$  current efficiency according to Eq. (10). Note: experimental energy consumption, as measured by a Kill-A-Watt monitor, was similar and ranged from  $0.63-1.25~\rm kWh.m^{-3}$ , see Table 1.

release of monovalent Mg ions, or the "chunk effect" as possible explanations for their high CE, while Brahmi et al. offered corrosion and anodic oxidation as explanation (Brahmi et al., 2019; Hug and Udert, 2013). There have not been extensive efforts to evaluate differences between theoretical and experimental electrode metal consumption, and many studies base the economic assessment solely on a theoretical analysis of measured current densities (Bayramoglu et al., 2007; Brahmi et al., 2019; Espinoza-Quiñones et al., 2009; Kobya and Demirbas, 2015; Kobya et al., 2016; Rodriguez et al., 2007). In these cases, the current is used to calculate the charge passed, and based upon an assumption that all of the charges go to metal corrosion, a theoretical metal consumption mass can then be calculated. On the other hand, our results suggest that this approach can severely underestimate the experimental mass of metal consumed and therefore the estimated materials costs. Furthermore, there are a few studies that compare economic and energy data across wastewater sources, and our results demonstrate that the energy consumption varies as a function of wastewater source, due to changes in water composition.

Operational costs also varied across treatments and methods of measurement, see Table 4. When using theoretical methods for measuring electricity and electrode consumption, expected costs ranged from 0.08  $\$.m^{-3}$  to 0.17  $\$.m^{-3}$  of treated wastewater with expected costs for the P-WW treatment being roughly double that of all other treatments, however, the experimentally measured values showed substantially different results. Operational costs across all treatments increased with values rising at a minimum of 59.5% for the P-WW treatment to a maximum increase of 185.2% for B-WW. Here, the treatment of B-WW sample was the most expensive with a cost of 0.30  $\$.\ m^{-3}.$ 

Due to P removal efficiencies varied across treatments, it is also useful to consider costs in terms of P removal. When viewed from this perspective, the P-WW treatment is the most cost effective with operational costs of 0.07~ \$.kg $^{-1}$  P removed, see Fig. 9. While theoretical

**Table 4**Operational costs evaluated for experimental and theoretical analysis methods.

| Cost Item                                     | P-WW  | F-WW   | FS-WW  | B-WW   |  |  |  |
|---|-------|--------|--------|--------|--|--|--|
| Energy Consumption Cost (\$.m <sup>-3</sup> ) |       |        |        |        |  |  |  |
| Experimental                                  | 0.09  | 0.04   | 0.04   | 0.04   |  |  |  |
| Theoretical                                   | 0.08  | 0.04   | 0.05   | 0.05   |  |  |  |
| Mg Consumption Cost (\$.m <sup>-3</sup> )     |       |        |        |        |  |  |  |
| Experimental                                  | 0.18  | 0.15   | 0.18   | 0.26   |  |  |  |
| Theoretical                                   | 0.09  | 0.04   | 0.06   | 0.06   |  |  |  |
| Total Operational Cost (\$.m <sup>-3</sup> )  |       |        |        |        |  |  |  |
| Experimental                                  | 0.27  | 0.19   | 0.22   | 0.30   |  |  |  |
| Theoretical                                   | 0.17  | 0.08   | 0.10   | 0.10   |  |  |  |
| Change in Cost (%)                            | 59.5% | 135.8% | 114.2% | 185.2% |  |  |  |

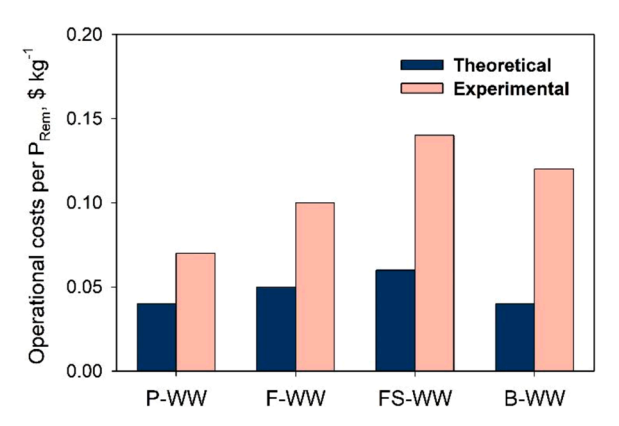


Fig. 9. The operational costs evaluated for theoretical and experimental analysis methods as per kg of phosphorus removed,  $P_{Rem}$ .

estimates would predict B-WW to show costs on par with the P-WW treatment, experimental results found costs to be 76.4% higher than P-WW (Fig. 9).

In a comparison to available literature, Abdel-Shafy  $\it et al.$  estimated operating costs of 0.88 \$.m $^{-3}$  for the treatment of cooling tower blowdown water using a magnesium-rod electrode, where they reported a phosphate removal efficiency of 98.0%, which is similar to P removal efficiencies seen with the P-WW treatment in our studies. On the other hand, while removal efficiencies were only 5.1% lower, operating costs for the P-WW treatment were 69.3% less than reported by Abdel-Shafy  $\it et al.$  Even with lower prices for electricity (\$0.04/kWh) and Mg (\$1.00/kg), higher consumption of energy, longer electrolysis times, and higher consumption of electrode material resulted in higher costs being realized in their study.

Studies utilizing Al as the sacrificial material report operating costs ranging from 0.27 \$.m<sup>-3</sup> (Lin et al., 2005) to 1.85 \$.m<sup>-3</sup> (Kobya et al., 2016). Studies utilizing Fe as the sacrificial material report operating costs ranging from 0.25 \$.m<sup>-3</sup> (Bayramoglu et al., 2007) to 1.70 \$.m<sup>-3</sup> (Espinoza-Quiñones et al., 2009). With experimental costs estimated in this study ranging from 0.19 \$.m<sup>-3</sup> to 0.30 \$.m<sup>-3</sup>, treatment under the conditions tested herein appears to be cost effective in relation to other studies utilizing Mg, Al, and Fe as a sacrificial material. Furthermore, as the majority of studies appear to use theoretical methods for estimating electrode consumption, our evaluation of *CE* reveals a likelihood that other studies may be underestimating the true costs associated with *EC* treatment.

# 4. Conclusions

In this study, we investigated the performance of a bench-scale electrochemical batch reactor for nutrient removal, as well as the electrochemical behavior of pure Mg disk electrodes in complex matrixes such as natural industrial or municipal wastewater sources. This work assessed the impact of the wastewater chemistry on Mg electrode corrosion behavior, anodic dissolution of Mg, and the kinetics and overall efficiency of nutrient removal. The scaled-up reactor removed up to 54% of the PO<sub>4</sub><sup>3-</sup> present in natural wastewaters within 1 min, with an energy input of 0.04 kWh.m<sup>3</sup> during that reaction time. Kinetic analysis showed that the PO<sub>4</sub><sup>3-</sup> removal followed a zero-order kinetic rate law for t > 1 min, and the rate constant (k) depended upon the total hardness (TH) and the levels of Cl<sup>-</sup>, NH<sub>4</sub><sup>+</sup>, and organic carbon present in the solution, with an inverse relationship between the rate constant and Ca<sup>2+</sup> ion concentration but a direct correlation between [Cl<sup>-</sup>] and [NH<sub>4</sub><sup>+</sup>] and the rate constant. The sacrificial anode showed the lowest corrosion resistance in the natural industrial wastewater source, while in the municipal wastewater sources, a general increase in the Tafel slope was observed. Surface characterization of the precipitate formed on the Mg anode during electrochemical treatment of P-WW indicated that the

film obtained on the anode surface was mainly magnesium hydroxide, presumed to form due to the increased bulk pH of wastewater source. The wastewater chemistry was impacted by the Mg<sup>2+</sup> dissolution where total dissolved solids (TDS) increased in the treated effluents. On the other hand, an overall improvement of water quality was observed based upon important water quality parameters such as total organic carbon (TOC), total suspended solids (TSS), and turbidity which all showed significant decreases. However, the electrochemically driven nutrient removal did not produce potable water directly. An economic assessment of the electrochemical results resulted in an estimated cost of 0.19 - 0.30 \$.m<sup>-3</sup>, based upon experimental Mg consumption data. Comparative results from the economic analysis showed the importance of basing costs on experimental Mg consumption data, as a theoretical basis is likely to underestimate costs. Furthermore, due to lower treatment times and Mg consumption rates, the estimated costs of this study are largely lower than those reported in the literature and are competitive with other electrocoagulation processes.

# **Declaration of Competing Interest**

None.

#### Acknowledgements

LKN, JP, LE, and LFG acknowledge the National Science Foundation (NSF) for this work's financial support through the INFEWS/T3 Award# 1739473 and the University of Arkansas Institute for Nanoscience and Nanotechnology characterization facility for support in surface and material characterization. ZA acknowledges support from the NSF Membrane Science, Engineering and Technology (MAST) I/UCRC. The authors thank John Askegaard for supplying natural wastewater samples of poultry condensate, Austin Ramsfield for supplying municipal wastewater samples from the West Side (Fayetteville, AR, USA) wastewater treatment facility, and Lance McAvoy for providing municipal wastewater samples from the P-Street (Fort Smith, AR, USA) and Massard (Barling, AR, USA) wastewater treatment facilities for testing. We are grateful to Andrew M. Herring, Professor of Chemical and Biological Engineering, Colorado School of Mines, for useful scientific discussions.

#### Supplementary materials

Supplementary material associated with this article can be found, in the online version, at doi:10.1016/j.watres.2021.118001.

#### References

- Abbasi, S., Aliofkhazraei, M., Mojiri, H., Amini, M., Ahmadzadeh, M., Shourgeshty, M., 2017. Corrosion behavior of pure Mg and AZ31 magnesium alloy. Protect. Metals Phys. Chem. Surfaces 53 (3), 573–578.
- Abdel-Shafy, H.I., Shoeib, M.A., El-Khateeb, M.A., Youssef, A.O., Hafez, O.M, 2020. Electrochemical treatment of industrial cooling tower blowdown water using magnesium-rod electrode. Wat. Res. Ind. 23, 100121.
- Abel-Denee, M., Abbott, T., Eskicioglu, C., 2018. Using mass struvite precipitation to remove recalcitrant nutrients and micropollutants from anaerobic digestion dewatering centrate. Water Res. 132, 292–300.
- Acelas, N.Y., Flórez, E., López, D., 2015. Phosphorus recovery through struvite precipitation from wastewater: effect of the competitive ions. Desalination Water Treat. 54 (9), 2468–2479.
- Agarwal, P., Crisalle, O.D., Orazem, M.E., Garcia-Rubio, L.H., 1995. Application of measurement models to impedance spectroscopy: II. Determination of the stochastic contribution to the error structure. J. Electrochem. Soc. 142 (12), 4149–4158.
- Bayramoglu, M., Eyvaz, M., Kobya, M., 2007. Treatment of the textile wastewater by electrocoagulation: economical evaluation. Chem. Eng. J. 128 (2), 155–161.
- Belarbi, Z., Trembly, J.P, 2018. Electrochemical processing to capture phosphorus from simulated concentrated animal feeding operations waste. J. Electrochem. Soc. 165 (13), E685–E693.
- Ben Moussa, S., Maurin, G., Gabrielli, C., Ben Amor, M., 2006. Electrochemical Precipitation of Struvite. Electrochem. Solid-State Lett. 9 (6), C97.
- Brahmi, K., Bouguerra, W., Hamrouni, B., Elaloui, E., Loungou, M., Tlili, Z., 2019. Investigation of electrocoagulation reactor design parameters effect on the removal of cadmium from synthetic and phosphate industrial wastewater. Arabian J. Chem. 12 (8), 1848–1859.

Cai, Y., Han, Z., Lin, X., Du, J., Lei, Z., Ye, Z., Zhu, J., 2021. Mechanisms of releasing magnesium ions from a magnesium anode in an electrolysis reactor with struvite precipitation. J. Environ. Chem. Eng., 106661

- Cai, Y., Han, Z., Lin, X., Duan, Y., Du, J., Ye, Z., Zhu, J., 2020. Study on removal of phosphorus as struvite from synthetic wastewater using a pilot-scale electrodialysis system with magnesium anode. Sci. Total Environ. 726, 138221.
- Coates, G., 1945. 124. The standard electrode potential of magnesium. J. Chem. Soc. (Resumed) 478–479.
- Cordell, D., Drangert, J.-O., White, S., 2009. The story of phosphorus: global food security and food for thought. Glob. Environ. Chang. 19, 292–305.
- Curioni, M., Scenini, F., Monetta, T., Bellucci, F., 2015. Correlation between electrochemical impedance measurements and corrosion rate of magnesium investigated by real-time hydrogen measurement and optical imaging. Electrochim. Acts 166, 272, 284.
- Curioni, M., Torrescano-Alvarez, J.M., Yang, Y.F., Scenini, F., 2016. Application of sideview imaging and real-time hydrogen measurement to the investigation of magnesium corrosion. Corrosion 73 (5), 463–470.
- Cusick, R.D., Logan, B.E, 2012. Phosphate recovery as struvite within a single chamber microbial electrolysis cell. Bioresour. Technol. 107, 110–115.
- Dura, A., Breslin, C.B, 2019. Electrocoagulation using aluminium anodes activated with Mg, In and Zn alloying elements. J. Hazard. Mater. 366, 39–45.
- Esmaily, M., Svensson, J.E., Fajardo, S., Birbilis, N., Frankel, G.S., Virtanen, S., Arrabal, R., Thomas, S., Johansson, L.G, 2017. Fundamentals and advances in magnesium alloy corrosion. Prog. Mater. Sci. 89, 92–193.
- Espinoza-Quiñones, F.R., Fornari, M.M.T., Módenes, A.N., Palácio, S.M., da Silva, F.G., Szymanski, N., Kroumov, A.D., Trigueros, D.E.G., 2009. Pollutant removal from tannery effluent by electrocoagulation. Chem. Eng. J. 151 (1), 59–65.
- Fischer, F., Bastian, C., Happe, M., Mabillard, E., Schmidt, N., 2011. Microbial fuel cell enables phosphate recovery from digested sewage sludge as struvite. Bioresour. Technol. 102 (10), 5824–5830.
- Gao, F., Wang, L., Wang, J., Zhang, H., Lin, S., 2020. Nutrient recovery from treated wastewater by a hybrid electrochemical sequence integrating bipolar membrane electrodialysis and membrane capacitive deionization. Environ. Sci. 6 (2), 383–391.
- Ge, F., Yin, J., Liu, Y., Leng, W., Wang, X., Cui, Z., 2021. Roles of pH in the NH4+-induced corrosion of AZ31 magnesium alloy in chloride environment. J. Magn. Alloys.
- Godfray, H.C.J., Beddington, J.R., Crute, I.R., Haddad, L., Lawrence, D., Muir, J.F., Pretty, J., Robinson, S., Thomas, S.M., Toulmin, C., 2010. Food Security: the Challenge of Feeding 9 Billion People. Science 327 (5967), 812–818.
- Govindan, K., Im, S.-.J., Muthuraj, V., Jang, A., 2021. Electrochemical recovery of H2 and nutrients (N, P) from synthetic source separate urine water. Chemosphere 269, 129361.
- Hug, A., Udert, K.M, 2013. Struvite precipitation from urine with electrochemical magnesium dosage. Water Res. 47 (1), 289–299.
- Ichihashi, O., Hirooka, K., 2012. Removal and recovery of phosphorus as struvite from swine wastewater using microbial fuel cell. Bioresour. Technol. 114, 303–307.
- Inan, H., Alaydın, E., 2014. Phosphate and nitrogen removal by iron produced in electrocoagulation reactor. Desalination Water Treat. 52 (7–9), 1396–1403.
- Kabdaszli, I., Parsons, S.A., Tünaya, O., 2006. Effect of major ions on induction time of struvite precipitation. Croat. Chem. Acta 79 (2), 243–251.
- Kékedy-Nagy, L., Abolhassani, M., Perez Bakovic, S.I., Anari, Z., Moore Ii, J.P., Pollet, B. G., Greenlee, L.F., 2020a. Electroless production of fertilizer (Struvite) and hydrogen from synthetic agricultural wastewaters. J. Am. Chem. Soc. 142 (44), 18844–18858.
- Kékedy-Nagy, L., Moore, J.P., Abolhassani, M., Attarzadeh, F., Hestekin, J.A., Greenlee, L.F, 2019. The passivating layer influence on Mg-based anode corrosion and implications for electrochemical struvite precipitation. J. Electrochem. Soc. 166 (12), E358–E364.
- Kékedy-Nagy, L., Teymouri, A., Herring, A.M., Greenlee, L.F., 2020b. Electrochemical removal and recovery of phosphorus as struvite in an acidic environment using pure magnesium vs. the AZ31 magnesium alloy as the anode. Chem. Eng. J. 380, 122480.
- Kekre, K.M., Anvari, A., Kahn, K., Yao, Y., Ronen, A., 2020. Reactive electrically conducting membranes for phosphorus recovery from livestock wastewater effluents. J. Environ. Manage., 111432
- Kim, J.H., An, B.m., Lim, D.H., Park, J.Y., 2018. Electricity production and phosphorous recovery as struvite from synthetic wastewater using magnesium-air fuel cell electrocoagulation. Water Res. 132, 200–210.
- Kim, K.-.W., Kim, Y.-.J., Kim, I.-.T., Park II, G., Lee, E.-.H, 2006. Electrochemical conversion characteristics of ammonia to nitrogen. Water Res. 40 (7), 1431–1441.
- Kobya, M., Demirbas, E., 2015. Evaluations of operating parameters on treatment of can manufacturing wastewater by electrocoagulation. J. Water Process Eng. 8, 64–74.
- Kobya, M., Gengec, E., Demirbas, E., 2016. Operating parameters and costs assessments of a real dyehouse wastewater effluent treated by a continuous electrocoagulation process. Chem. Eng. Process. 101, 87–100.
- Kreżel, A., Bal, W., 2004. A formula for correlating pKa values determined in D2O and H2O. J. Inorg. Biochem. 98 (1), 161–166.
- Kruk, D.J., Elektorowicz, M., Oleszkiewicz, J.A., 2014. Struvite precipitation and phosphorus removal using magnesium sacrificial anode. Chemosphere 101, 28–33.
- Lahav, O., Telzhensky, M., Zewuhn, A., Gendel, Y., Gerth, J., Calmano, W., Birnhack, L., 2013. Struvite recovery from municipal-wastewater sludge centrifuge supernatant using seawater NF concentrate as a cheap Mg(II) source. Sep. Purif. Technol. 108, 103–110.
- Le Corre, K.S., Valsami-Jones, E., Hobbs, P., Parsons, S.A, 2005. Impact of calcium on struvite crystal size, shape and purity. J. Cryst. Growth 283 (3), 514–522.
- Lei, Y., Geraets, E., Saakes, M., van der Weijden, R.D., Buisman, C.J.N, 2020. Electrochemical removal of phosphate in the presence of calcium at low current density: precipitation or adsorption? Water Res. 169, 115207.

182, 24-38,

Lei, Y., Remmers, J.C., Saakes, M., van der Weijden, R.D., Buisman, C.J.N, 2019. Influence of cell configuration and long-term operation on electrochemical phosphorus recovery from domestic wastewater. ACS Sustain Chem. Eng. 7 (7), 7362–7368.

- Lei, Y., Zhan, Z., Saakes, M., van der Weijden, R.D., Buisman, C.J.N, 2021. Electrochemical Recovery of Phosphorus from Acidic Cheese Wastewater: Feasibility, Quality of Products, and Comparison with Chemical Precipitation. ACS ES&T Water.
- Li, B., Boiarkina, I., Young, B., Yu, W., 2016. Quantification and mitigation of the negative impact of calcium on struvite purity. Adv. Powder Technol. 27 (6), 2354–2362.
- Li, X., Zhao, X., Zhou, X., Yang, B., 2021. Phosphate recovery from aqueous solution via struvite crystallization based on electrochemical-decomposition of nature magnesite. J. Clean. Prod. 292, 126039.
- Liao, M., Liu, Y., Tian, E., Ma, W., Liu, H., 2020. Phosphorous removal and high-purity struvite recovery from hydrolyzed urine with spontaneous electricity production in Mg-air fuel cell. Chem. Eng. J. 391, 123517.
- Lin, C.-.J., Lo, S.-.L., Kuo, C.-.Y., Wu, C.-.H, 2005. Pilot-scale electrocoagulation with bipolar aluminum electrodes for on-site domestic greywater reuse. J. Environ. Eng. 131 (3), 491–495.
- Lin, X., Han, Z., Yu, H., Ye, Z., Zhu, S., Zhu, J., 2018. Struvite precipitation from biogas digestion slurry using a two-chamber electrolysis cell with a magnesium anode. J. Clean. Prod. 174, 1598–1607.
- Liu, W., Li, J., He, X., Wang, Z., Chun, Z., 2019. Factors influencing the removal of phosphorus and the purity of recycling struvite in wastewater by the electrochemical sacrificial magnesium anode method. Sci. Adv. Mater. 11 (1), 128–134.
- Martínez, L.M.P., Ramón, M.V.L., Cámara, M.A.F., Castilla, M., 2010. Batch and column adsorption of herbicide fluroxypyr on different types of Removal of Organics From Aqueous Solution 529 activated carbons from water with varied egrees of hardness and alkalinity. Water Res. 44, 879–885.
- Massey, M.S., Davis, J.G., Ippolito, J.A., Sheffield, R.E, 2009. Effectiveness of recovered magnesium phosphates as fertilizers in neutral and slightly alkaline soils. Agronomy J. 101 (2), 323–329.
- Naresh Kumar, A., Bandarapu, A.K., Venkata Mohan, S., 2019. Microbial electrohydrolysis of sewage sludge for acidogenic production of biohydrogen and volatile fatty acids along with struvite. Chem. Eng. J. 374, 1264–1274.
- Nasr, M., Ateia, M., Hassan, K., 2016. Artificial intelligence for greywater treatment using electrocoagulation process. Sep. Sci. Technol. 51 (1), 96–105.
- Orazem, M.E., 2004. A systematic approach toward error structure identification for impedance spectroscopy. J. Electroanal. Chem. 572 (2), 317–327.
- Rabinovich, A., Rouff, A.A, 2021. Effect of Phenolic Organics on the Precipitation of Struvite from Simulated Dairy Wastewater. ACS ES&T Water 1 (4), 910–918.
- Rasmussen, L.V., Coolsaet, B., Martin, A., Mertz, O., Pascual, U., Corbera, E., Dawson, N., Fisher, J.A., Franks, P., Ryan, C.M, 2018. Social-ecological outcomes of agricultural intensification. Nat. Sustain. 1 (6), 275.
- Ren, S., Li, M., Sun, J., Bian, Y., Zuo, K., Zhang, X., Liang, P., Huang, X., 2017. A novel electrochemical reactor for nitrogen and phosphorus recovery from domestic wastewater. Front. Environ. Sci. Eng. 11 (4), 17.
- Rodriguez, J., Stopić, S., Krause, G., Friedrich, B., 2007. Feasibility assessment of electrocoagulation towards a new sustainable wastewater treatment. Environ. Sci. Pollut. Res. - Int. 14 (7), 477–482.
- Shen, Y., Arogo Ogejo, J., Bowers, K., 2010. Reducing the Effects of Calcium on Struvite Precipitation in Liquid Dairy Manure. ASABE. St. Joseph, MI.
- Shu, J., Wu, H., Chen, M., Peng, H., Li, B., Liu, R., Liu, Z., Wang, B., Huang, T., Hu, Z., 2019. Fractional removal of manganese and ammonia nitrogen from electrolytic metal manganese residue leachate using carbonate and struvite precipitation. Water Res. 153, 229–238.
- Shu, L., Schneider, P., Jegatheesan, V., Johnson, J., 2006. An economic evaluation of phosphorus recovery as struvite from digester supernatant. Bioresour. Technol. 97 (17), 2211–2216.

- Shukla, P.K., Orazem, M.E., Crisalle, O.D, 2004. Validation of the measurement model concept for error structure identification. Electrochim. Acta 49 (17), 2881–2889.
  Stoll, V.S., Blanchard, J.S., 1990. [4]Buffers: principles and practice. Meth. Enzymol.
- Szpyrkowicz, L., Naumczyk, J., Zilio-Grandi, F., 1995. Electrochemical treatment of tannery wastewater using TiPt and Ti/Pt/Ir electrodes. Water Res. 29 (2), 517–524.
- Tan, X., Yu, R., Yang, G., Wei, F., Long, L., Shen, F., Wu, J., Zhang, Y., 2020. Phosphate recovery and simultaneous nitrogen removal from urine by electrochemically induced struvite precipitation. Environ. Sci. Pollut. Res.
- Tilman, D., Balzer, C., Hill, J., Befort, B.L, 2011. Global food demand and the sustainable intensification of agriculture. Proc. Natl. Acad. Sci. U.S.A 108 (50), 20260–20264.
- US EIA, 2021. Table 5.3 Average Price of Electricity to Ultimate Customers: Year to Date, 2021. U.S. Energy Information Administration. https://www.eia.gov/electricity/monthly/epm\_table\_grapher.php?t=epmt\_5\_03. Accessed 22 October 2021.
- USGS, 2021. Magnesium Metal. Mineral Commodity Summaries 2021. Geological Survey, U.S.. https://doi.org/10.3133/mcs2021. Accessed 22 October 2021.
- Vanlangendonck, Y., Corbisier, D., Van Lierde, A., 2005. Influence of operating conditions on the ammonia electro-oxidation rate in wastewaters from power plants (ELONITA™ technique). Water Res. 39 (13), 3028–3034.
- Wang, F., Fu, R., Lv, H., Zhu, G., Lu, B., Zhou, Z., Wu, X., Chen, H., 2019a. Phosphate recovery from swine wastewater by a struvite precipitation electrolyzer. Sci. Rep. 9 (1), 8893.
- Wang, F., Fu, R., Lv, H., Zhu, G., Lu, B., Zhou, Z., Wu, X., Chen, H., 2019b. Phosphate recovery from swine wastewater by a struvite precipitation electrolyzer. Sci. Rep. 9 (1), 8893.
- Wang, F., Wei, J., Zou, X., Fu, R., Li, J., Wu, D., Lv, H., Zhu, G., Wu, X., Chen, H., 2019c. Enhanced electrochemical phosphate recovery from livestock wastewater by adjusting pH with plant ash. J. Environ. Manage. 250, 109473.
- Williams, G., Neil McMurray, H., 2008. Localized corrosion of magnesium in chloridecontaining electrolyte studied by a scanning vibrating electrode technique. J. Electrochem. Soc. 155 (7), C340.
- Wu, I., Teymouri, A., Park, R., Greenlee, L.F., Herring, A.M, 2019. Simultaneous electrochemical nutrient recovery and hydrogen generation from model wastewater using a sacrificial magnesium anode. J. Electrochem. Soc. 166 (16), E576.
- Yan, H., Shih, K., 2016. Effects of calcium and ferric ions on struvite precipitation: a new assessment based on quantitative X-ray diffraction analysis. Water Res. 95, 310–318.
- Yan, J., Springsteen, G., Deeter, S., Wang, B., 2004. The relationship among pKa, pH, and binding constants in the interactions between boronic acids and diols—It is not as simple as it appears. Tetrahedron 60 (49), 11205–11209.
- Yao, J., Zhou, M., Wen, D., Xue, Q., Wang, J., 2016. Electrochemical conversion of ammonia to nitrogen in non-chlorinated aqueous solution by controlling pH value. J. Electroanal. Chem. 776, 53–58.
- Zeng, F., Zhao, Q., Jin, W., Liu, Y., Wang, K., Lee, D.-.J., 2018. Struvite precipitation from anaerobic sludge supernatant and mixed fresh/stale human urine. Chem. Eng. J. 344, 254–261.
- Zhang, D., Zeng, K., 2012. Evaluating the behavior of electrolytic gas bubbles and their effect on the cell voltage in alkaline water electrolysis. Ind. Eng. Chem. Res. 51 (42), 13825–13832.
- Zhang, Z., She, L., Zhang, J., Wang, Z., Xiang, P., Xia, S., 2019. Electrochemical acidolysis of magnesite to induce struvite crystallization for recovering phosphorus from aqueous solution. Chemosphere 226, 307–315.
- Zhou, Z., Hu, D., Ren, W., Zhao, Y., Jiang, L.-M., Wang, L., 2015. Effect of humic substances on phosphorus removal by struvite precipitation. Chemosphere 141, 04.00
- Zöllig, H., Fritzsche, C., Morgenroth, E., Udert, K.M, 2015. Direct electrochemical oxidation of ammonia on graphite as a treatment option for stored source-separated urine. Water Res. 69, 284–294.